Journal of Sound and Vibration (1999) **219**(5), 813–835
Article No. jsvi.1998.1890, available online at http://www.idealibrary.com on IDEAL

EFFECTS OF SUBTENDED AND VERTEX ANGLES ON THE FREE VIBRATION OF OPEN CONICAL SHELL PANELS: A CONICAL CO-ORDINATE APPROACH

C. W. LIM

Department of Mechanical Engineering, *The University of Hong Kong*, *Pokfulam Road*, *Hong Kong*

AND

S. KITIPORNCHAI

Department of Civil Engineering, *The University of Queensland*, *Brisbane*, *Queensland* 4072, *Australia*

(*Received* 27 *April* 1998, *and in final form* 30 *July* 1998)

The paper presents a computational investigation on the effects of subtended and vertex angles on the free vibration characteristics of open conical shell panels. Unlike the conventional approximation using a rectangular or cylindrical co-ordinate system, this analysis adopts a natural conical co-ordinate system so that any approximation in geometry is eliminated. The strain and curvature components formulated in this orthogonal conical co-ordinate system have been employed to derive the strain and kinetic energy integrals. The energy functional is minimized in accordance with the Ritz procedure to arrive at a governing eigenvalue equation. Admissible shape functions comprising sets of two-dimensional orthogonal polynomials and a basic function are employed to account for the boundary constraints and to approximate the three-dimensional displacements of the conical shell. Comparison of natural frequencies shows excellent agreement with the solutions of finite element, finite strip and integral equation methods. The effects of subtended and vertex angles and other geometric parameters on vibration are investigated in a comprehensive parametric study. Selected vibration mode shapes are illustrated to enhance the physical understanding of vibration of such open conical shell panels.

1. INTRODUCTION

There has been extensive use of conical shell panels and conical frustums in various engineering applications such as aircraft structures, turbomachinery blades, cooling towers and jet nozzles. The vibration characteristics are of critical importance to the performance and safety of these structures. A thorough

0022–460X/99/050813 + 23 $30.00/0

analytical understanding of the resonant properties of these shells is therefore significant and important.

In respect of turbomachinery blades, the conical shell panel has rarely been used as a model in analysis [1–6] although as an approximation it is much superior to the conventional beam, plate and shallow shell models. Actual turbomachinery blades feature not only pretwist and thickness variation, but most importantly spanwise variable radius and variable deep curvature. Conventional models including beams, plates and shallow shells can be formulated to incorporate the effects of pretwist and thickness variation [7–17], but it is impossible to include spanwise variable radius and curvature due to the geometric deficiency of the models. Most early works employed a one-dimensional beam theory approach [1–3] which is only justifiable provided the structures are slender or only lower vibration modes are required. The two-dimensional plate and shallow shell models with and without pretwist and thickness variation have been reported in numerous publications [4–17]. These analyses, however, neglected the variable radius and variable deep surface curvature. Although a general variable strain and change of curvature formulation has been presented by Lee *et al*. [18], numerical solutions presented were restricted to plates and cylindrical shells with zero and constant surface curvature. To the authors' knowledge, the only reported conical shell modelling of turbomachinery blades has been by Lim and Liew and their co-workers [19–24]. Unfortunately, these are *shallow* conical shell analyses which are geometrically insufficient in a realistic and rigorous effort to model an actual turbomachinery blade. As a result, a conical shell model featuring variable radius, deepness and variable curvature is inevitable to realistically model turbomachinery blades.

On the other hand, there have been several studies of the vibration analysis of closed conical shells [6, 7, 25, 26]. Despite the practical importance, there are very few references dealing with open conical shell panels. Besides the authors' work on shallow conical shell panels [19–24], vibration solutions for open conical shell panels have been presented by Srinivasan and Krishnan [27] using an integral equation approach; by Cheung *et al*. [28] using a spline finite strip method; and by Lim *et al*. [29] using a Ritz method in a conical co-ordinate system. This paper, in fact, is an extension of the paper presented by Lim *et al*. [29] at the Fifth Pan American Congress of Applied Mechanics.

The fact that there are relatively few publications on the free vibration analysis of open conical shell panels is partly due to the mathematical complexity in geometry and partly due to the variable large surface curvature. However, mathematical and geometry complexity only arise if a non-natural co-ordinate system, such as the Cartesian co-ordinate system, is adopted. To account for this difficulty, a natural conical co-ordinate system similar to that of Leissa and So [26] is used to derive the strain and curvature components based on the shell theory of Gol'denveizer [30] and Novozhilov [31]. The strain and kinetic energy integrals in this conical system are formulated and the Ritz energy functional is minimized to derive a governing eigenvalue equation. A set of admissible p-Ritz shape functions [15–17, 19–24, 29, 32, 33] is introduced to approximate the transverse and in-plane displacement amplitude functions. These shape functions are

composed of the product of sets of two-dimensional polynomials and appropriate basic functions. The basic functions are associated with piecewise boundary expressions of the structure raised to an appropriate basic power and satisfy the geometric boundary conditions at the outset. Consequently, this approach is highly versatile in accommodating various boundary conditions. Unlike the finite element and finite strip methods, numerical formulation and computational implementation can be greatly simplified because no mesh generation is needed. Furthermore, only relatively small amounts of computational memory and execution time are required and yet accurate solutions can be achieved.

In this study, the consistency of the numerical approach is verified through a convergence study to demonstrate the existence of upperbound eigenvalues. A comparison study with some available data and finite element solutions is included to authenticate the accuracy and reliability of the present approach. To enhance existing literature, a comprehensive set of first known non-dimensional frequency parameters is presented showing the effects of subtended and vertex angles on free vibration of open conical shell panels. Selected vibration mode shapes are also illustrated to visualize the displacement amplitude.

2. ENERGY FUNCTIONAL

Consider a homogeneous, isotropic, thin open conical shell panel with slanting length of panel (or reference length) l_0, slanting length of cone $(L + l_0)$, thickness h, reference radius R_0 perpendicular to the conical midsurface (not in the plane of cone base) as the normal distance from conical midsurface to the cone axis, half vertex angle θ_v and subtended angle θ_0 as shown in Figure 1. An orthogonal conical co-ordinate system (r, θ, l) is defined whether r is the normal distance from the conical midsurface parallel to R, θ is the circumferential angle measured in a plane perpendicular to the cone axis, and l is the distance from a reference point of midsurface along a meridian. The displacements of the conical midsurface are

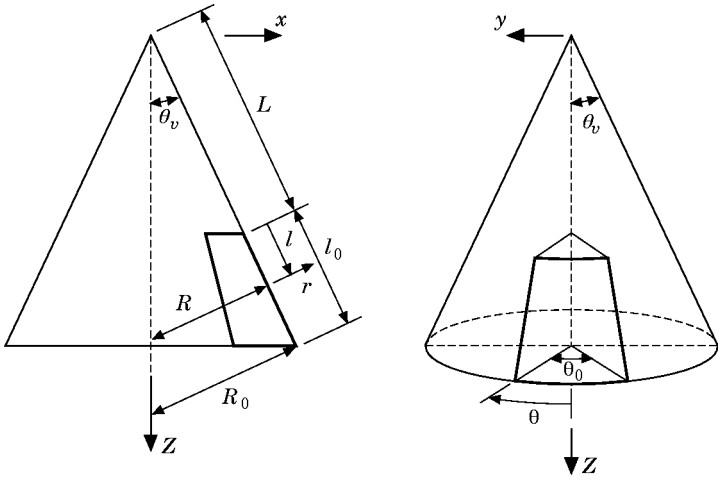

Figure 1. Geometry of a conical shell panel.

resolved into three orthogonal components u_r, u_θ and u_l. The radius R varies linearly with respect to l and the relation is

$$R = R_o - (l_o - l)\tan\theta_v. \tag{1}$$

From the strain–displacement expressions of Gol'denveizer [30] and Novozhilov [31] which is valid for an arbitrary orthogonal coordinate system and deepness of shell, the following strain– and curvature–displacement relationships are derived,

$$\epsilon_\theta = \frac{1}{R\cos\theta_v}\frac{\partial u_\theta}{\partial\theta} + \frac{\tan\theta_v}{R}u_l + \frac{u_r}{R}, \qquad \epsilon_l = \frac{\partial u_l}{\partial l}, \tag{2.1, 2}$$

$$\epsilon_{\theta l} = \frac{1}{R\cos\theta_v}\frac{\partial u_l}{\partial\theta} + \frac{\partial u_\theta}{\partial l} - \frac{\tan\theta_v}{R}u_\theta, \tag{2.3}$$

$$\kappa_\theta = \frac{1}{R^2\cos\theta_v}\frac{\partial u_\theta}{\partial\theta} - \frac{1}{R^2\cos^2\theta_v}\frac{\partial^2 u_r}{\partial\theta^2} - \frac{\tan\theta_v}{R}\frac{\partial u_r}{\partial l}, \qquad \kappa_l = -\frac{\partial^2 u_r}{\partial l^2}, \tag{2.4, 5}$$

$$\tau = \frac{1}{R}\frac{\partial u_\theta}{\partial l} - \frac{\tan\theta_v}{R^2}u_\theta - \frac{1}{R\cos\theta_v}\frac{\partial^2 u_r}{\partial\theta\,\partial l} + \frac{\tan\theta_v}{R^2\cos\theta_v}\frac{\partial u_r}{\partial\theta}. \tag{2.6}$$

For small amplitude vibration, the total strain energy, U, is given by [7, 18, 31]

$$U = U_s + U_b, \tag{3}$$

where U_s is the membrane stretching strain energy and U_b is the bending strain energy. The strain energy components can be expressed as

$$U_s = \frac{6D}{h^2}\iint_A\left[\epsilon_\theta^2 + \epsilon_l^2 + 2\nu\epsilon_\theta\epsilon_l + \frac{1-\nu}{2}\epsilon_{\theta l}^2\right]R\cos\theta_v\,\mathrm{d}\theta\,\mathrm{d}l, \tag{4.1}$$

$$U_b = \frac{D}{2}\iint_A\Big[\kappa_\theta^2 + \kappa_l^2 + 2\nu\kappa_\theta\kappa_l + 2(1-\nu)\tau^2\Big]R\cos\theta_v\,\mathrm{d}\theta\,\mathrm{d}l, \tag{4.2}$$

where the flexural rigidity $D = Eh^3/12(1-\nu^2)$, E is Young's modulus, and ν the Poisson's ratio. The double integration above covers the entire conical midsurface A.

The kinetic energy is given by [7, 18, 31]

$$T = \frac{\rho h}{2}\iint_A\left[\left(\frac{\partial u_\theta}{\partial t}\right)^2 + \left(\frac{\partial u_l}{\partial t}\right)^2 + \left(\frac{\partial u_r}{\partial t}\right)^2\right]R\cos\theta_v\,\mathrm{d}\theta\,\mathrm{d}l, \tag{5}$$

where ρ is the mass density per unit volume.

For a non-dissipative system, the maximum stretching strain components in a vibrating cycle can be derived by substituting equations (2.1–6) into equations (4.1, 2) as

$$(U_s)_{max} = \frac{6D}{h^2}\iint\left\{\frac{1}{R\cos\theta_v}\left(\frac{\partial U_\theta}{\partial\theta}\right)^2 + \frac{\sin\theta_v\tan\theta_v}{R}U_l^2 + \frac{\cos\theta_v}{R}U_r^2\right.$$

$$+\frac{2\tan\theta_v}{R}\frac{\partial U_\theta}{\partial\theta}U_l + \frac{2}{R}\frac{\partial U_\theta}{\partial\theta}U_r + \frac{2\sin\theta_v}{R}U_lU_r + R\cos\theta_v\left(\frac{\partial U_l}{\partial l}\right)^2$$

$$+2\nu\left[\frac{\partial U_\theta}{\partial\theta}\frac{\partial U_l}{\partial l} + \sin\theta_v U_l\frac{\partial U_l}{\partial l} + \cos\theta_v\frac{\partial U_l}{\partial l}U_r\right]$$

$$+\frac{1-\nu}{2}\left[\frac{1}{R\cos\theta_v}\left(\frac{\partial U_l}{\partial\theta}\right)^2 + R\cos\theta_v\left(\frac{\partial U_\theta}{\partial l}\right)^2 + \frac{\sin\theta_v\tan\theta_v}{R}U_\theta^2\right.$$

$$\left.\left.+2\frac{\partial U_\theta}{\partial l}\frac{\partial U_l}{\partial\theta} - \frac{2\tan\theta_v}{R}U_\theta\frac{\partial U_l}{\partial\theta} - 2\sin\theta_v U_\theta\frac{\partial U_\theta}{\partial l}\right]\right\}\mathrm{d}\theta\,\mathrm{d}l, \tag{6.1}$$

$$(U_b)_{max} = \frac{D}{2}\iint\left\{\frac{1}{R^3\cos\theta_v}\left(\frac{\partial U_\theta}{\partial\theta}\right)^2 + \frac{1}{R^3\cos^3\theta_v}\left(\frac{\partial^2 U_r}{\partial\theta^2}\right)^2 + \frac{\sin\theta_v\tan\theta_v}{R}\left(\frac{\partial U_r}{\partial l}\right)^2\right.$$

$$-\frac{2}{R^3\cos^2\theta_v}\frac{\partial U_\theta}{\partial\theta}\frac{\partial^2 U_r}{\partial\theta^2} - \frac{2\tan\theta_v}{R^2}\frac{\partial U_\theta}{\partial\theta}\frac{\partial U_r}{\partial l}$$

$$+\frac{2\tan\theta_v}{R^2\cos\theta_v}\frac{\partial^2 U_r}{\partial\theta^2}\frac{\partial U_r}{\partial l} + R\cos\theta_v\left(\frac{\partial^2 U_r}{\partial l^2}\right)^2 + 2\nu\left[-\frac{1}{R}\frac{\partial U_\theta}{\partial\theta}\frac{\partial^2 U_r}{\partial l^2}\right.$$

$$\left.+\frac{1}{R\cos\theta_v}\frac{\partial^2 U_r}{\partial\theta^2}\frac{\partial^2 U_r}{\partial l^2} + \sin\theta_v\frac{\partial U_r}{\partial l}\frac{\partial^2 U_r}{\partial l^2}\right]$$

$$+2(1-\nu)\left[\frac{\cos\theta_v}{R}\left(\frac{\partial U_\theta}{\partial l}\right)^2 - \frac{2\sin\theta_v}{R^2}U_\theta\frac{\partial U_\theta}{\partial l} + \frac{\sin\theta_v\tan\theta_v}{R^3}U_\theta^2\right.$$

$$-\frac{2}{R}\frac{\partial U_\theta}{\partial l}\frac{\partial^2 U_r}{\partial\theta\,\partial l} + \frac{2\tan\theta_v}{R^2}\frac{\partial U_\theta}{\partial l}\frac{\partial U_r}{\partial\theta} + \frac{2\tan\theta_v}{R^2}U_\theta\frac{\partial^2 U_r}{\partial\theta\,\partial l}$$

$$-\frac{2\tan^2\theta_v}{R^3}U_\theta\frac{\partial U_r}{\partial\theta} + \frac{1}{R\cos\theta_v}\left(\frac{\partial^2 U_r}{\partial\theta\,\partial l}\right)^2$$

$$\left.\left.-\frac{2\tan\theta_v}{R^2\cos\theta_v}\frac{\partial U_r}{\partial\theta}\frac{\partial^2 U_r}{\partial\theta\,\partial l} + \frac{\tan^2\theta_v}{R^3\cos\theta_v}\left(\frac{\partial U_r}{\partial\theta}\right)^2\right]\right\}\mathrm{d}\theta\,\mathrm{d}l, \tag{6.2}$$

while the maximum kinetic energy in a vibrating cycle is

$$T_{max} = \frac{\rho h \omega^2 \cos\theta_v}{2} \iint R(U_\theta^2 + U_l^2 + U_r^2)\, \mathrm{d}\theta\, \mathrm{d}l \tag{7}$$

where ω is the angular frequency.

The displacement amplitude functions $U_\theta(\theta, l)$, $U_l(\theta, l)$ and $U_r(\theta, l)$ can be approximated by the following two-dimensional polynomial functions

$$U_\theta(\theta, s) = \sum_{i=1}^{m} C_\theta^i \phi_\theta^i(\theta, l), \qquad U_l(\theta, l) = \sum_{i=1}^{m} C_l^i \phi_l^i(\theta, l), \tag{8.1, 2}$$

$$U_r(\theta, l) = \sum_{i=1}^{m} C_r^i \phi_r^i(\theta, l), \tag{8.3}$$

where C_θ^i, C_l^i and C_r^i are the unknown coefficients and ϕ_θ^i, ϕ_l^i and ϕ_r^i are the corresponding p-Ritz shape functions to be introduced in due course.

For simplicity and generality, a non-dimensional conical midsurface co-ordinate system $(\overline{\theta}, \overline{l})$ is further introduced as

$$\overline{\theta} = \theta/\theta_0, \qquad \overline{l} = l/l_0, \tag{9.1, 2}$$

such that $\overline{\theta}$ and $\overline{l}$ range from $[-0{\cdot}5, 0{\cdot}5]$ and $[0, 1]$ respectively. The displacement amplitude functions (8.1–3) can be expressed in these non-dimensional co-ordinates. Similarly, the strain and kinetic energy components in equations (6.1, 2) and (7) can also be expressed in these non-dimensional conical midsurface co-ordinates.

In accordance with the Ritz procedure, an energy functional Π defined as

$$\Pi = U_{max} - T_{max} \tag{10}$$

is minimized with respect to the unknown coefficients

$$\partial\Pi/\partial C_\alpha^i = 0; \qquad \alpha = \theta,\ l \text{ and } r, \tag{11}$$

which yields a governing eigenvalue equation as follows

$$(\mathbf{K} - \lambda^2 \mathbf{M})\{\mathbf{C}\} = \{\mathbf{0}\}, \tag{12}$$

where

$$\lambda = \omega l_0^2 \sqrt{\rho h / D} \tag{13}$$

is the non-dimensional frequency parameter. The stiffness and mass matrices are

$$\mathbf{K} = \begin{bmatrix} k_{\theta\theta} & k_{\theta l} & k_{\theta r} \\ & k_{ll} & k_{lr} \\ \text{sym} & & k_{rr} \end{bmatrix}, \qquad \mathbf{M} = \begin{bmatrix} M_{\theta\theta} & [0] & [0] \\ & m_{ll} & [0] \\ \text{sym} & & m_{rr} \end{bmatrix} \tag{14, 15}$$

and the vector of unknown coefficients is

$$\mathbf{C} = \begin{Bmatrix} \{C_\theta\}_j \\ \{C_l\} \\ \{C_r\} \end{Bmatrix}, \tag{16}$$

where the elements in the stiffness matrix are

$$k_{\theta\theta}^{ij} = \frac{6l_0^2}{h^2}\left[\frac{2\eta^2}{\theta_0^2} I_{\theta\theta}^{ij(1010;-1)} + (1-\nu) I_{\theta\theta}^{ij(0101;1)} + (1-\nu)\eta^2 \sin^2\theta_v I_{\theta\theta}^{ij(0000;-1)} - (1-\nu)\eta \sin\theta_v (I_{\theta\theta}^{ij(0100;0)} + I_{\theta\theta}^{ij(0001;0)})\right] + \frac{l_0^2\eta^2}{R_0^2\theta_0^2} I_{\theta\theta}^{ij(1010;-3)} + \frac{2(1-\nu)l_0^2}{R_0^2}[I_{\theta\theta}^{ij(0101;-1)} - \eta \sin\theta_v (I_{\theta\theta}^{ij(0100;-2)} + I_{\theta\theta}^{ij(0001;-2)}) + \eta^2 \sin^2\theta_v I_{\theta\theta}^{ij(0000;-3)}], \tag{17.1}$$

$$k_{\theta l}^{ij} = \frac{6l_0^2\eta}{h^2\theta_0}[2\eta \sin\theta_v I_{\theta l}^{ij(1000;-1)} + 2\nu I_{\theta l}^{ij(1001;0)} + (1-\nu) I_{\theta l}^{ij(0110;0)} - (1-\nu)\eta \sin\theta_v I_{\theta l}^{ij(0010;-1)}] \tag{17.2}$$

$$k_{\theta r}^{ij} = \frac{12l_0^3\eta}{h^2 R_0\theta_0} I_{\theta r}^{ij(1000;-1)} - \frac{l_0\eta^2}{R_0\theta_0}\left[\frac{\eta}{\theta_0^2} I_{\theta r}^{ij(1020;-3)} + \sin\theta_v I_{\theta r}^{ij(1001;-2)}\right] - \frac{\nu l_0\eta}{R_0\theta_0} I_{\theta r}^{ij(1002;-1)} + \frac{2(1-\nu)l_0\eta}{R_0\theta_0}[-I_{\theta r}^{ij(0111;-1)} + \eta \sin\theta_v I_{\theta r}^{ij(0110;-2)} + \eta \sin\theta_v I_{\theta r}^{ij(0011;-2)} - \eta^2 \sin^2\theta_v I_{\theta r}^{ij(0010;-3)})], \tag{17.3}$$

$$k_{ll}^{ij} = \frac{6l_0^2}{h^2}\left[2\eta^2 \sin^2\theta_v I_{ll}^{ij(0000;-1)} + 2I_{ll}^{ij(0101;1)} + 2\nu\eta \sin\theta_v (I_{ll}^{ij(0100;0)} + I_{ll}^{ij(0001;0)}) + \frac{(1-\nu)\eta^2}{\theta_0^2} I_{ll}^{ij(1010;-1)}\right], \tag{17.4}$$

$$k_{lr}^{ij} = \frac{12l_0^3}{h^2 R_0}[\eta \sin\theta_v I_{lr}^{ij(0000;-1)} + \nu I_{lr}^{ij(0100;0)}], \tag{17.5}$$

$$k_{rr}^{ij} = \frac{12I_0^4}{h^2R_0^2} I_{rr}^{ij(0000;-1)} + \frac{\eta^4}{\theta_0^4} I_{rr}^{ij(2020;-3)} + \eta^2 \sin^2\theta_v I_{rr}^{ij(0101;-1)} + \frac{\eta^3 \sin\theta_v}{\theta_0^2}(I_{rr}^{ij(2001;-2)}$$

$$+ I_{rr}^{ij(0120;-2)}) + I_{rr}^{ij(0202;1)} + \frac{v\eta^2}{\theta_0^2}(I_{rr}^{ij(0220;-1)} + I_{rr}^{ij(2002;-1)})$$

$$+ v\eta \sin\theta_v (I_{rr}^{ij(0201;0)} + I_{rr}^{ij(0102;0)}) + \frac{2(1-v)\eta^2}{\theta_0^2}[I_{rr}^{ij(1111;-1)}$$

$$- \eta \sin\theta_v (I_{rr}^{ij(1011;-2)} + I_{rr}^{ij(1110;-2)}) + \eta^2 \sin^2\theta_v I_{rr}^{ij(1010;-3)}]. \tag{17.6}$$

and the elements in the mass matrix are

$$m_{\theta\theta}^{ij} = I_{\theta\theta}^{ij(0000;1)}, \qquad m_{\theta l}^{ij} = 0, \qquad m_{\theta r}^{ij} = 0, \qquad m_{ll}^{ij} = I_{ll}^{ij(0000;1)}, \tag{18.1–4}$$

$$m_{lr}^{ij} = 0, \qquad m_{rr}^{ij} = I_{rr}^{ij(0000;1)}, \tag{18.5, 6}$$

in which

$$\eta = \frac{l_0}{R_0 \cos\theta_v}, \qquad I_{\alpha\beta}^{ij(abcd;e)} = \int\int_{\bar{A}} \frac{\partial^{a+b}\phi_\alpha^i(\bar{\theta},\bar{l})}{\partial\bar{\theta}^a\,\partial\bar{l}^b} \frac{\partial^{c+d}\phi_\beta^j(\bar{\theta},\bar{l})}{\partial\bar{\theta}^c\,\partial\bar{l}^d} \bar{R}^e \,\mathrm{d}\bar{\theta}\,\mathrm{d}\bar{l}, \tag{19.1, 2}$$

where $\bar{A}$ is the normalized conical midsurface area;

$$\bar{R} = 1 - (l_0/R_0)(1-\bar{l})\tan\theta_v \tag{20}$$

is the dimensionless radius; $\alpha, \beta = \theta, l, r$; $i, j = 1, 2, \ldots, m$ and m is the total number of terms employed in the p-Ritz shape functions. The derivatives of strain and kinetic energy integrals with respect to the unknown coefficients for equation (11) are derived in the Appendix.

3. ADMISSIBLE SHAPE FUNCTIONS

The displacement components in midsurface denoted by U_θ, U_l and U_r are approximated by a finite series given in equations (8.1–3). Their corresponding admissible shape functions ϕ_θ, ϕ_l and ϕ_r are sets of geometrically compliant two-dimensional polynomials derived such that the geometric boundary conditions are satisfied at the outset. They are composed of the product of a series of simple two-dimensional polynomials F_0 and boundary compliant basic functions ϕ_α^b ($\alpha = \theta$, l and r). The latter are geometric expressions of the conical panel boundary raised to an appropriate basic power in accordance with various boundary constraints. Accordingly, the admissible shape functions are

$$\phi_\alpha = F_0(\bar{\theta},\bar{l})\phi_\alpha^b, \qquad F_0(\bar{\theta},\bar{l}) = \sum_{q=0}^{p}\sum_{i=0}^{q} \bar{\theta}^{q-i}\bar{l}^i, \qquad \alpha = \theta,\ l \text{ or } r \tag{21.1–3}$$

where p is the highest degree of polynomial in the functions, m is the number of terms and they are related by $m = (p+1)(p+2)/2$. The series F_0 can be determined easily by constructing a Pascal polynomial triangle [32].

For convenience, F, S and C are used to denote free, simply supported and clamped boundaries respectively. A CSFC shell represents a shell panel with two clamped boundaries along $\overline{\theta} = -0{\cdot}5$ and $\overline{l} = 1{\cdot}0$; a simply supported boundary along $\overline{l} = 0$; and a free boundary along $\overline{\theta} = 0{\cdot}5$. For conical shell panels with symmetric geometry and boundary constraints, it is possible to classify the vibration modes into two symmetry classes with respect to the *lr*-plane. For instance, the vibration modes of a fully clamped CCCC conical panel can be classified into symmetric (S) and antisymmetric (A) modes. As a result, $F_0(\overline{\theta}, \overline{l})$ can be subdivided into odd and even functions in terms of powers of $\overline{\theta}$:

$$F_0(\overline{\theta}, \overline{l}) = F_1(\overline{\theta}_e, \overline{l}) + F_2(\overline{\theta}_0, \overline{l}), \tag{22}$$

where $\overline{\theta}_e$ and $\overline{\theta}_0$ denote polynomial functions with even and odd powers of $\overline{\theta}$ respectively, and

$$F_1(\overline{\theta}_e, \overline{l}) = \sum_{q=0}^{p} \sum_{i=0,2,4,\ldots}^{q} \overline{\theta}^i \overline{l}^{q-i}, \qquad F_2(\overline{\theta}_o, \overline{l}) = \sum_{q=0}^{p} \sum_{i=1,3,5,\ldots}^{q} \overline{\theta}^i \overline{l}^{q-i}. \tag{23.1, 2}$$

The corresponding admissible shape functions are

$$\phi_\alpha = F_1(\overline{\theta}_e, \overline{l})\phi_\alpha^b; \qquad \text{symmetric wrt } lr\text{-plane;} \tag{24.1}$$

$$\phi_\alpha = F_2(\overline{\theta}_0, \overline{l})\phi_\alpha^b; \qquad \text{antisymmetric wrt } lr\text{-plane;} \tag{24.2}$$

where $\alpha = \theta$, l or r.

The subdivision of two-dimensional functions according to various symmetry classes for the displacements has been presented by Lim *et al*. [32, 33]. The corresponding number of terms for each symmetry class with respect to the highest polynomial power has also been tabulated [32, 33].

The boundary compliant basic functions ϕ_α^b ($\alpha = \theta$, l or r) are defined as the product of the equations of continuous piecewise boundary geometries raised to an appropriate basic power that corresponds to the type of boundary constraint, i.e.,

$$\phi_\theta^b(\overline{\theta}, \overline{l}) = \prod_{i=1}^{4} [\Upsilon_i(\overline{\theta}, \overline{l})]^{\gamma_\theta^i}, \qquad \gamma_\theta^i = \begin{Bmatrix} 0 & \text{free;} \\ 1 & \text{simply supported or clamped;} \end{Bmatrix} \tag{25.1}$$

$$\phi_l^b(\overline{\theta}, \overline{l}) = \prod_{i=1}^{4} [\Upsilon_i(\overline{\theta}, \overline{l})]^{\gamma_l^i}, \qquad \gamma_l^i = \begin{Bmatrix} 0 & \text{free;} \\ 1 & \text{simply supported or clamped;} \end{Bmatrix}, \tag{25.2}$$

$$\phi_r^b(\overline{\theta}, \overline{l}) = \prod_{i=1}^{4} [\Upsilon_i(\overline{\theta}, \overline{l})]^{\gamma_r^i}, \qquad \gamma_r^i = \begin{Bmatrix} 0 & \text{free;} \\ 1 & \text{simply supported;} \\ 2 & \text{clamped.} \end{Bmatrix}, \tag{25.3}$$

TABLE 1

Convergence and comparison of $\lambda = \omega l_0^2\sqrt{(\rho h/D)}$ *for a fully clamped deep conical shell panel with* $\nu = 0{\cdot}3$, $l_0/(L + l_0) = 0{\cdot}6$ *and* $l_0/h = 100$

			Mode sequence number							
θ_v	θ_0	p	S-1	S-2	S-3	S-4	A-1	A-2	A-3	A-4
30°	30°	9	399·58	470·93	546·30	626·27	491·66	631·42	767·63	915·36
		11	399·57	470·91	546·20	625·65	491·51	630·53	764·16	900·32
		13	399·57	470·91	546·19	625·58	491·51	630·48	763·38	897·30
		15	399·57	470·91	546·19	625·57	491·50	630·47	763·31	897·06
		60 × 60†	398·22	468·26	541·95	619·28	484·71	618·86	746·08	873·22
	45°	9	341·01	413·20	479·85	481·34	275·97	381·65	481·54	582·70
		11	341·01	413·18	479·71	481·26	275·95	381·26	479·26	578·62
		13	341·01	413·18	479·70	481·25	275·95	381·24	479·16	578·02
		15	341·01	413·18	479·70	481·25	275·95	381·24	479·15	577·96
		60 × 60†	339·15	411·03	475·85	478·10	274·21	377·75	473·34	569·14
	60°	9	256·55	351·26	401·37	435·30	209·73	307·80	400·00	423·91
		11	256·54	351·21	401·22	435·14	209·71	307·60	397·89	420·90
		13	256·54	351·21	401·21	435·13	209·71	307·59	397·71	420·52
		15	256·54	351·21	401·21	435·12	209·71	307·59	397·70	420·50
		60 × 60†	254·84	348·22	399·87	431·53	208·99	305·83	394·54	416·15
		7 × 7‡	266·1	358·3	–	–	195·1	300·7	399·3	–
		9 × 9‡	260·1	355·0	–	–	202·7	305·6	402·9	–
		8 × 6§	263·7	361·5	–	–	214·2	317·6	–	–
		12 × 6§	262·5	358·6	–	–	213·4	314·7	–	–
45°	30°	9	237·55	289·94	347·36	410·62	276·89	374·35	470·89	573·28
		11	237·54	289·93	347·34	410·52	276·87	374·05	469·99	570·01
		13	237·54	289·93	347·34	410·52	276·86	374·04	469·95	569·54
		15	237·54	289·93	347·34	410·52	276·86	374·04	469·94	569·49
		60 × 60†	237·05	288·92	345·61	407·67	274·71	369·98	463·46	559·99
	45°	9	202·37	257·07	277·20	309·58	166·30	241·36	315·96	371·96
		11	202·37	257·07	277·17	309·57	166·30	241·32	315·32	370·61
		13	202·37	257·07	277·17	309·57	166·30	241·32	315·29	370·45
		15	202·37	257·07	277·17	309·57	166·30	241·32	315·28	370·43
		60 × 60†	201·62	256·23	275·85	308·32	165·72	240·00	312·86	366·64
	60°	9	153·61	223·76	239·28	282·44	137·43	207·64	242·71	278·56
		11	153·61	223·74	239·23	282·43	137·42	207·44	241·31	278·10
		13	153·61	223·74	239·23	282·43	137·42	207·44	241·23	278·06
		15	153·60	223·74	239·23	282·43	137·42	207·44	241·23	278·06
		60 × 60†	153·01	222·56	238·70	281·49	137·17	206·62	239·81	276·56

† NASTRAN finite element solutions; ‡ Srinivasan and Krishnan [27], integral equation approach; § Cheung *et al*. [28], finite strip method.

where Υ_i is the geometric boundary expression of the ith supporting edge. For instance, the basic functions for a CCCC open conical panel are

$$\phi_\theta^b = (\overline{\theta}^2 - 0{\cdot}25)\overline{l}(\overline{l} - 1), \qquad \phi_l^b = (\overline{\theta}^2 - 0{\cdot}25)\overline{l}(\overline{l} - 1), \tag{26.1, 2}$$

$$\phi_r^b = (\overline{\theta}^2 - 0{\cdot}25)^2\,\overline{l}^2(\overline{l} - 1)^2. \tag{26.3}$$

4. RESULTS AND DISCUSSION

Table 1 presents a convergence and comparison study of vibration frequencies for a fully clamped (CCCC) open conical shell panel. Vibration solutions of this panel were obtained by Srinivasan and Krishnan [27] using an integral equation approach and by Cheung *et al*. [28] using a spline finite strip method. To demonstrate the convergence of eigenvalues, the degree of polynomial functions in equations (23.1, 2) has been increased from 9 to 15. For symmetric modes as governed by equation (23.1), the total number of terms is $m = 30$ for $p = 9$ and $m = 72$ for $p = 15$ while for antisymmetric modes $m = 25$ and $m = 64$ respectively. If no classification of modes is performed, $m = 136$ would be needed for $p = 15$. It has been investigated by Lim *et al*. [32, 33] that tremendous numerical effort (ranging from 40% to 65% for single symmetry classification) can be saved accounting for the total execution period for both cases.

Downward convergence of eigenvalues is demonstrated in Table 1. It is expected because the Ritz method always overestimates stiffness, vibration frequency and buckling load and underestimates deflection. Accurate solutions can be obtained by including an adequate number of terms in the admissible polynomial shape functions. As observed in Table 1, $p = 15$ is able to justify converged eigenvalues up to four significant digits in most cases. Consequently, $p = 15$ has been used in all subsequent numerical computation. Table 1 also exhibits excellent agreement between solutions obtained by Srinivasan and Krishnan [27] and Cheung *et al*. [28] using different numerical methods. It is obvious that convergence of solutions of Srinivasan and Krishnan [27] and Cheung *et al*. [28] is not very satisfactory as can be seen in Table 1 for the two different meshes. To further verify the accuracy of the current conical co-ordinate approach, finite element solutions have been obtained using NASTRAN with 60×60 4-noded plate elements. Convergence of finite element solutions has been tested and, again, excellent agreement of solutions has been demonstrated.

Another comparison of non-dimensional frequency parameter λ with the solutions of Cheung *et al*. [28] is presented in Figures 2 and 3 for a CCCC conical shell panel with $v = 0{\cdot}3$, $(L + l_0)/h = 400$, $\theta_0 = 30^\circ$, $\theta_v = 30^\circ$ and 45°, respectively. The frequency modes have been classified as symmetric (S) or antisymmetric (A) with respect to the *lr*-plane in accordance with equation (24.1, 2). Two modes in each class have been shown in the figures. It should be emphasized that numerical solutions of Cheung *et al*. [28] are not available but rather the results were presented in graphical logarithmic scales. Direct hand measurement from the figures was extremely crude and, therefore, the authors would suggest a 5–10% measurement tolerance. Comparison of solutions within a 10% difference would be deemed acceptable. In these figures, excellent agreement of solutions is achieved considering the crude data extracted manually from Cheung *et al*. [28].

In another comparison in Figure 4, NASTRAN finite element solutions have been obtained using 4-noded plate elements for a conical shell panel with $v = 0{\cdot}3$, $l_0/h = 100$, $\theta_0 = 30^\circ$ and $\theta_v = 30^\circ$. Different mesh sizes have been employed in the finite element analysis with meshes 60×30 for $l_0/(L + l_0) = 0{\cdot}2$; 60×40 for $l_0/(L + l_0) = 0{\cdot}3$; 60×50 for $l_0/(L + l_0) = 0{\cdot}4$; and 60×60 for $l_0/(L + l_0) = 0{\cdot}5$, $0{\cdot}6$, $0{\cdot}7$ and $0{\cdot}8$. Although the mesh size varies, convergence of finite element

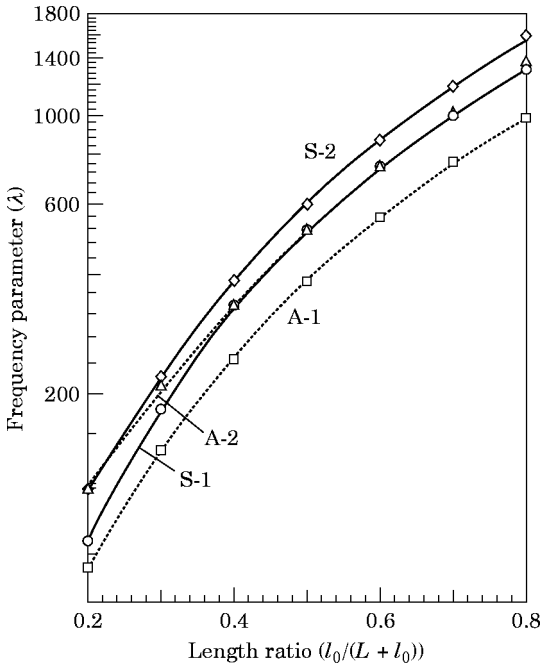

Figure 2. Comparison of frequency parameter λ for a CCCC conical shell panel with $\nu = 0{\cdot}3$, $(L + l_0)/h = 400$, $\theta_0 = 30^\circ$ and $\theta_v = 30^\circ$. Key for Cheung *et al*. results [28]: ○, S-1; ◇, S-2; □, A-1; △, A-2.

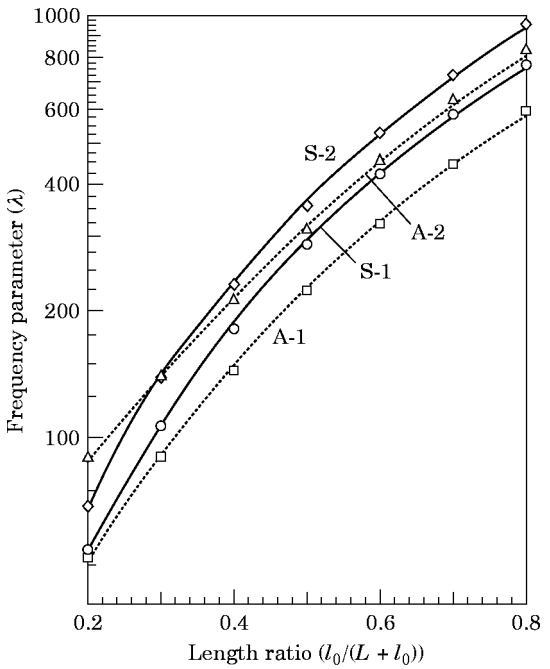

Figure 3. Comparison of frequency parameter λ for a CCCC conical shell panel with $\nu = 0{\cdot}3$, $(L + l_0)/h = 400$, $\theta_0 = 30^\circ$ and $\theta_v = 45^\circ$. Key as for Figure 2.

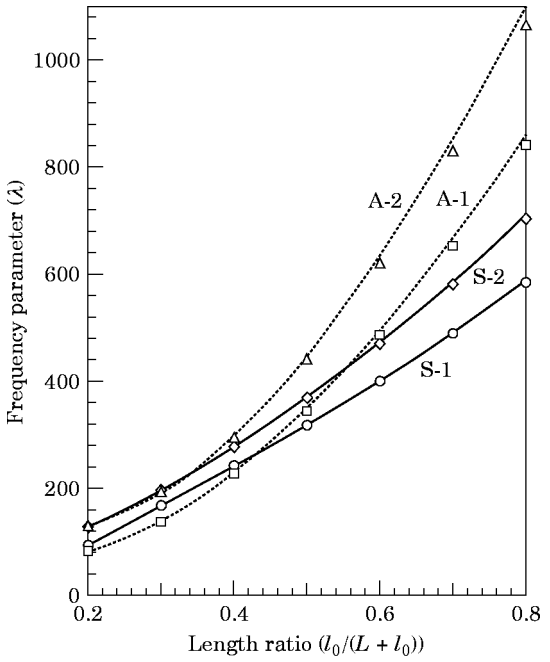

Figure 4. Comparison of frequency parameter λ for a CCCC conical shell panel with $v = 0{\cdot}3$, $l_0/h = 100$, $\theta_0 = 30^\circ$ and $\theta_v = 30^\circ$. Key for FEM solution (NASTRAN) as for Figure 2.

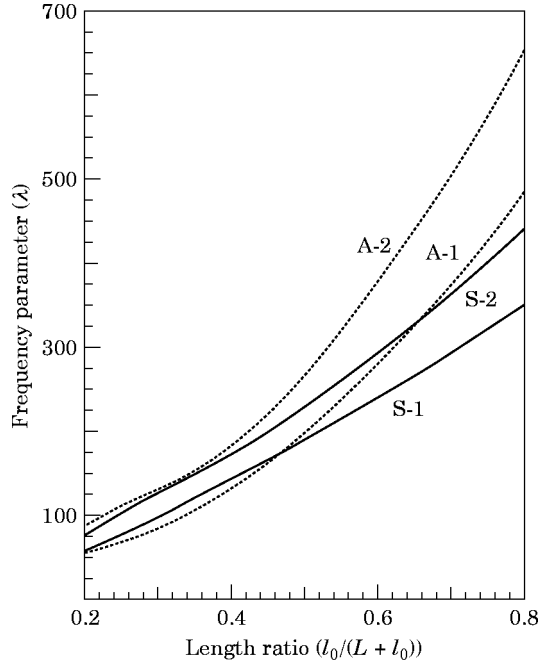

Figure 5. Frequency parameter λ for a CCCC conical shell panel with $v = 0{\cdot}3$, $l_0/h = 100$, $\theta_0 = 30^\circ$ and $\theta_v = 45^\circ$.

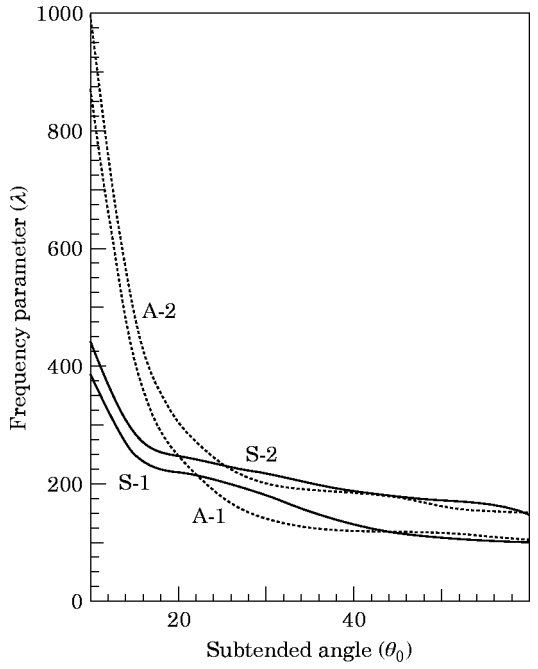

Figure 6. Frequency parameter λ for a CCCC conical shell panel with $\nu = 0{\cdot}3$, $l_0/(L + l_0) = 0{\cdot}3$, $(L + l_0)/h = 400$ and $\theta_v = 30^\circ$.

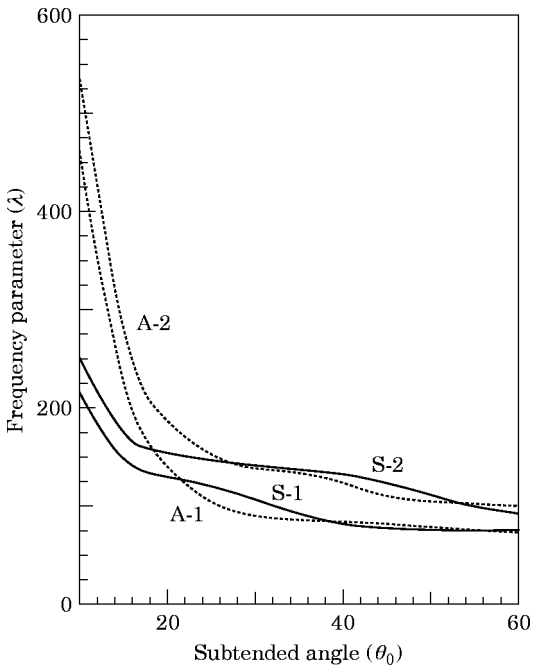

Figure 7. Frequency parameter λ for a CCCC conical shell panel with $\nu = 0{\cdot}3$, $l_0/(L + l_0) = 0{\cdot}3$, $(L + l_0)/h = 400$ and $\theta_v = 45^\circ$.

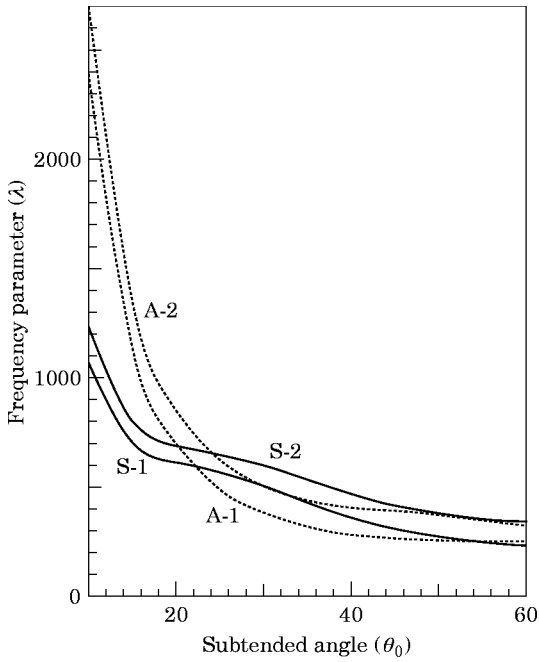

Figure 8. Frequency parameter λ for a CCCC conical shell panel with $\nu = 0{\cdot}3$, $l_0/(L + l_0) = 0{\cdot}5$, $(L + l_0)/h = 400$ and $\theta_v = 30^\circ$.

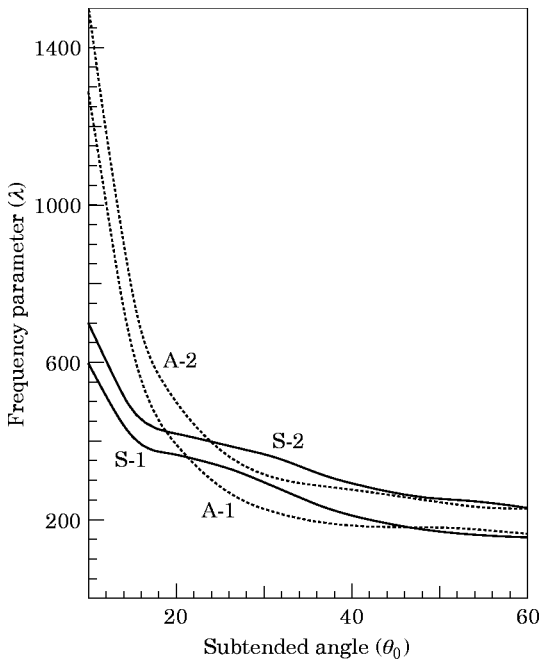

Figure 9. Frequency parameter λ for a CCCC conical shell panel with $\nu = 0{\cdot}3$, $l_0/(L + l_0) = 0{\cdot}5$, $(L + l_0)/h = 400$ and $\theta_v = 45^\circ$.

solutions has been checked in all cases. Again, excellent comparison of solutions has been achieved.

The effects of varying cone length and vertex angle can be observed in Figures 4 and 5 which present the non-dimensional frequency parameter for open conical shell panels with $v = 0{\cdot}3$, $l_0/h = 100$, $\theta_0 = 30^\circ$, $\theta_v = 30^\circ$ and 45°, respectively. The physical thickness h is not unchanging but rather the thickness ratio l_0/h is constant while $l_0/(L + l_0)$ is varying. For a conical panel with a smaller vertex angle ($2\theta_v = 60^\circ$), the fundamental vibration mode is antisymmetric (A-1) with respect to the lr-plane when the panel is short ($l_0/(L + l_0) = 0{\cdot}2$). This fundamental mode switches from antisymmetric (A-1) to symmetric (S-1) when the panel becomes longer, or, when $l_0/(L + l_0)$ gradually increases from 0·2 to 0·8. The crossing of the lowest symmetric and antisymmetric modes occurs at $l_0/(L + l_0) \approx 0{\cdot}44$. Because all sides of the shell panel are clamped, it implies that it is too stiff for a short conical shell panel ($l_0/(L + l_0) < 0{\cdot}44$ approximately) with $2\theta_v = 60^\circ$ to vibrate in a half-wavelength mode (S-1) than a full-wavelength mode (A-1) in the circumferential θ-direction, as can be seen in vibration mode shape diagrams discussed in due course. For a long conical shell panel ($l_0/(L + l_0) > 0{\cdot}44$ approximately), it is more flexible to vibrate in a half-wavelength mode (S-1) than a full-wavelength mode (A-1) in the circumferential θ direction. Not all S-1 vibration modes correspond to one half-wavelength mode and not all A-1 vibration modes correspond to one full-wavelength mode (equivalent to two half-wavelengths) as they could correspond to odd multiples of half-wavelengths (such as 3 half-wavelengths) and even multiples of half-wavelengths (such as 4 half-wavelengths). Examples will be illustrated in vibration mode shapes figures.

Similar trends have also been observed in Figure 5 for a conical panel with a large vertex angle ($2\theta_v = 90^\circ$). The switching of the lowest symmetric and

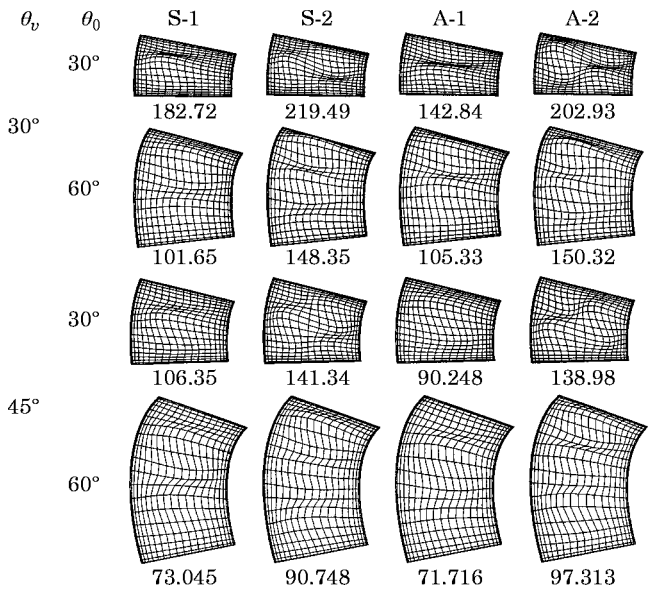

Figure 10. Vibration frequencies and mode shapes for a CCCC conical shell panel with $v = 0{\cdot}3$, $l_0/(L + l_0) = 0{\cdot}3$ and $(L + l_0)/h = 400$.

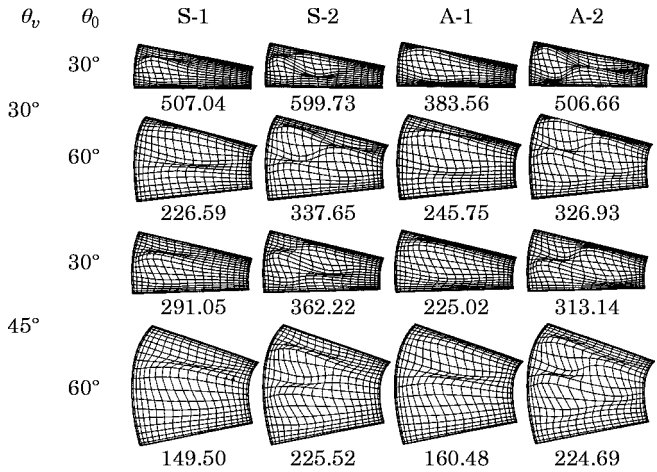

Figure 11. Vibration frequencies and mode shapes for a CCCC conical shell panel with $\nu = 0{\cdot}3$, $l_0/(L + l_0) = 0{\cdot}5$ and $(L + l_0)/h = 400$.

antisymmetric modes occurs at $l_0/(L + l_0) \approx 0{\cdot}46$. From Figures 4 and 5, it can also be deduced that the fundamental λ (either S-1 or A-1) is higher for a conical shell panel with a smaller vertex angle. In other words, increasing the vertex angle decreases the vibration frequency parameters.

For conical shell panels with constant physical thickness h, the effects of changing the vertex (θ_v) and subtended (θ_0) angles are presented in Figures 6–9. It is apparent that in all cases the fundamental modes are symmetric for conical panels with a small θ_0 ($= 10^\circ$) and these fundamental modes switch from symmetric to antisymmetric at $\theta_0 \approx 22^\circ$. The fundamental modes again switch back to symmetric modes at a larger angle depending on the shell geometry. Apparently, λ for all vibration modes decreases when θ_0 increases implying a less stiff wider panel compared to a narrower panel. Comparing Figures 6 ($\theta_v = 30^\circ$) and 7 ($\theta_v = 45^\circ$) as well as Figures 8 ($\theta_v = 30^\circ$) and 9 ($\theta_v = 45^\circ$), the frequency parameters are generally higher for conical panels with a smaller vertex angle. From Figures 6 ($l_0/(L + l_0) = 0{\cdot}3$) and 8 ($l_0/(L + l_0) = 0{\cdot}5$) as well as Figures 7 ($l_0/(L + l_0) = 0{\cdot}3$) and 9 ($l_0/(L + l_0) = 0{\cdot}5$), it is again observed that a longer conical shell panel has higher vibration frequencies.

A set of vibration frequencies and midsurface displacement amplitude mode shapes for a CCCC conical shell panel with $\nu = 0{\cdot}3$, $(L + l_0)/h = 400$, $l_0/(L + l_0) = 0{\cdot}3$ and $0{\cdot}5$ is illustrated in Figures 10 and 11, respectively. Symmetric (S) and antisymmetric (A) mode shapes with respect to the lr-plane can be observed. Four modes corresponding to S-1, S-2, A-1 and A-2 modes are illustrated. Nodal lines with zero vibration amplitude can be observed. For instance, the S-1 and S-2 modes with $\theta_v = 30^\circ$ and $\theta_0 = 30^\circ$ have no nodal line and one spanwise (θ-direction) nodal line, respectively, while the corresponding A-1 and A-2 modes have one lengthwise (l-direction) nodal line and two nodal lines (one lengthwise and one spanwise), respectively. The number of nodal lines increases for higher vibration modes. As discussed above, not all fundamental modes correspond to either a half-wavelength or a full-wavelength in the spanwise

or circumferential direction. This phenomenon happens especially when the subtended angle is large ($\theta_0 = 60^\circ$). An example for the S-1 mode with $\theta_v = 30^\circ$ and $\theta_0 = 60^\circ$ is observed in Figure 10 where it has three spanwise half-wavelengths while the corresponding A-1 mode has two spanwise full-wavelengths.

5. CONCLUSIONS

A new approach using an orthogonal conical co-ordinate system in conjunction with the Ritz extremum energy method has been formulated to investigate the free vibration of open conical shell panels. Expressions for strain–displacement, curvature–displacement relationships and strain–kinetic energy functional have been derived in this conical co-ordinate system. The kinematically oriented p-Ritz shape functions previously developed in plate and shell analyses in Cartesian co-ordinate system by the authors have been extended to this conical co-ordinate system. Geometric and mathematical deficiency and complexity in conventional co-ordinate systems dealing with conical panels have been completely eliminated as this new and natural conical co-ordinate system presents an exact geometric representation.

Convergence of eigenvalues has been verified and excellent agreement has been achieved with available published data and NASTRAN finite element solutions. The effects of length ratio, vertex and subtended angles have also been examined and discussed. A set of new results for a wide range of subtended angle and length ratio has been presented. It is not necessary for a fundamental symmetric (or antisymmetric) mode to vibrate in a one half-wavelength (or one full-wavelength) mode in the circumferential direction and the nature of vibration modes depends on the vertex angle. Furthermore, the fundamental mode also switches from a symmetric mode to an antisymmetric mode, or *vice versa*, depending on the cone length, subtended and vertex angles. It has been observed that there is a tendency for an open conical panel with a larger vertex angle to vibrate with a lower frequency parameter. To enhance the physical understanding of vibration modes, selected displacement amplitude mode shapes have been illustrated and analysed.

ACKNOWLEDGMENTS

A research fellowship for the first author from The University of Hong Kong and the Australian Research Council Small Grant 98/ARCS070G of The University of Queensland are gratefully acknowledged.

REFERENCES

1. J. S. Rao 1973 *The Shock and Vibration Digest* **5**(10), 3–16. Natural frequencies of turbine blading—a survey.
2. J. S. Rao 1977 *The Shock and Vibration Digest* **9**(3), 15–22. Turbine blading excitation and vibration.
3. J. S. Rao 1980 *The Shock and Vibration Digest* **12**(2), 19–26. Turbomachine blade vibration.

4. A. W. Leissa 1980 *The Shock and Vibration Digest* **12**(11), 3–10. Vibrations of turbine engine blades by shell analysis.
5. A. W. Leissa 1981 *Applied Mechanics Reviews* **34**, 629–635. Vibrational aspects of rotating turbomachinery blades.
6. K. M. Liew, C. W. Lim and S. Kitipornchai 1997 *Applied Mechanics Reviews* **50**, 431–444. Various theories for vibration of shallow shells: a review with bibliography.
7. A. W. Leissa 1973 *NASA SP*-288. Vibration of shells.
8. A. W. Leissa, J. C. MacBain and R. E. Kielb 1984 *Journal of Sound and Vibration* **96**, 159–173. Vibrations of twisted cantilevered plates—summary of previous and current studies.
9. J. C. MacBain, R. E. Kielb and A. W. Leissa 1985 *Transactions of the ASME Journal of Engineering for Gas Turbines and Power* **107**, 187–196. Vibration of twisted cantilevered plates—experimental investigation.
10. R. E. Kielb, A. W. Leissa and J. C. MacBain 1985 *International Journal for Numerical Methods in Engineering* **21**, 1365–1380. Vibrations of twisted cantilevered plates—a comparison of theoretical results.
11. M. D. Olson and G. M. Lindberg 1971 *Journal of Sound and Vibration* **19**, 299–318. Dynamic analysis of shallow shells with a doubly-curved triangular finite element.
12. K. P. Walker 1978 *Journal of Sound and Vibration* **59**, 35–57. Vibrations of cambered helicoidal fan blades.
13. A. W. Leissa, J. K. Lee and A. J. Wang 1982 *Transactions of the ASME Journal of Engineering for Power* **104**, 296–302. Rotating blade vibration analysis using shells.
14. A. W. Leissa and M. S. Ewing 1983 *Transactions of the ASME Journal of Engineering for Power* **105**, 383–392. Comparison of beam and shell theories for the vibrations of thin turbomachinery blades.
15. C. W. Lim and K. M. Liew 1994 *Journal of Sound and Vibration* **173**, 343–375. A *pb*-2 Ritz formulation for flexural vibration of shallow cylindrical shells of rectangular planform.
16. K. M. Liew and C. W. Liew 1994 *American Institute of Aeronautics and Astronautics Journal* **32**, 387–396. Vibratory characteristics of cantilevered rectangular shallow shells of variable thickness.
17. C. W. Lim and K. M. Liew 1995 *Acta Mechanica* **111**, 193–208. Vibration of pretwisted cantilever trapezoidal symmetric laminates.
18. J. K. Lee, A. W. Leissa and A. J. Wang 1984 *Transactions of the ASME Journal of Engineering for Gas Turbines and Power* **106**, 11–16. Vibrations of blades with variable thickness and curvature by shell theory.
19. C. W. Lim and K. M. Liew 1995 *Engineering Structures* **17**, 63–70. Vibratory behaviour of shallow conical shells by a global Ritz formulation.
20. K. M. Liew, M. K. Lim, C. W. Lim, D. B. Li and Y. R. Zhang 1995 *Journal of Sound and Vibration* **180**, 271–296. Effects of initial twist and thickness variation on the vibration behaviour of shallow conical shells.
21. C. W. Lim, S. Kitipornchai and K. M. Liew 1996 *The Sixth International Symposium on Transport Phenomena and Dynamics of Rotating Machinery*, I, 227–236 (edited by D. C. Han, S. T. Ro and J. H. Kim), 25–28 February, Honolulu, U.S.A. Vibration of pretwisted cantilever shallow conical shells of non-uniform cross-section.
22. C. W. Lim and K. M. Liew 1996 *International Journal of Solids and Structures* **33**, 451–468. Vibration of shallow conical shells with shear flexibility: a first order theory.
23. C. W. Lim, K. M. Liew and S. Kitipornchai 1997 *American Institute of Aeronautics and Astronautics Journal* **35**, 327–333. Effects of pretwist and fibre orientation on vibration of cantilevered composite shallow conical shells.
24. C. W. Lim, K. M. Liew and S. Kitipornchai 1998 *International Journal of Solids and Structures* **35**, 1695–1707. Vibration of cantilevered laminated composite shallow conical shells.

25. C. H. CHANG 1981 *The Shock and Vibration Digest* **13**(6), 9–17. Vibration of conical shells.
26. A. W. LEISSA and J. SO 1995 *Journal of Vibration and Control* **1**, 145–158. Three-dimensional vibrations of truncated hollow cones.
27. R. S. SRINIVASAN and P. A. KRISHNAN 1987 *Journal of Sound and Vibration* **117**, 153–160. Free vibration of conical shell panels.
28. Y. K. CHEUNG, W. Y. LI and L. G. THAM 1989 *Journal of Sound and Vibration* **128**, 411–422. Free vibration analysis of singly curved shell by spline finite strip method.
29. C. W. LIM, K. M. LIEW and S. KITIPORNCHAI 1997 *Fifth Pan American Congress on Applied Mechanics* (edited by L. A. Godoy, M. Rysz and L. E. Suárez), 2–4 January San Juan, Puerto Rico, U.S.A. **4**, 306–309. Vibrations of deep conical shell panels using a conical coordinate system.
30. A. L. GOL'DENVEIZER 1961 *Theory of Thin Shells*. New York: Pergamon Press.
31. V. V. NOVOZHILOV 1959 *The Theory of Thin Shells*. Groningen: P. Noordhoff.
32. C. W. LIM, K. M. LIEW and S. KITIPORNCHAI 1998 *Computer Methods in Applied Mechanics and Engineering* **156**, 15–29. Numerical aspects for free vibration of thick plates. Part I: formulation and verification.
33. C. W. LIM, S. KITIPORNCHAI and K. M. LIEW 1998 *Computer Methods in Applied Mechanics and Engineering* **156**, 31–44. Numerical aspects for free vibration of thick plates. Part II: numerical efficiency and vibration frequencies.

APPENDIX

The derivatives of strain and kinetic energy integrals with respect to the unknown coefficients for equation (11) are as follows

$$\frac{\partial(U_s)_{max}}{\partial C_\theta^i} = \frac{6D}{h^2}\left\{\frac{2\eta}{\theta_0}\left(\sum_{j=1}^{m} C_\theta^j I_{\theta\theta}^{ij(1010;-1)}\right) + 2\eta \sin\theta_v\left(\sum_{j=1}^{m} C_l^j I_{\theta l}^{ij(1000;-1)}\right)\right.$$

$$+ \frac{2l_0}{R_0}\left(\sum_{j=1}^{m} C_r^j I_{\theta r}^{ij(1000;-1)}\right) + 2v\left(\sum_{j=1}^{m} C_l^j I_{\theta l}^{ij(1001;0)}\right)$$

$$+ (1-v)\left[\frac{\theta_0}{\eta}\left(\sum_{j=1}^{m} C_\theta^j I_{\theta\theta}^{ij(0101;1)}\right) + \theta_0\eta \sin^2\theta_v\left(\sum_{j=1}^{m} C_\theta^j I_{\theta\theta}^{ij(0000;-1)}\right)\right.$$

$$+ \left(\sum_{j=1}^{m} C_l^j I_{\theta l}^{ij(0110;0)}\right) - \eta \sin\theta_v\left(\sum_{j=1}^{m} C_l^j I_{\theta l}^{ij(0010;-1)}\right)$$

$$\left.\left. - \theta_0 \sin\theta_v\left(\sum_{j=1}^{m} C_\theta^j (I_{\theta\theta}^{ij(0100;0)} + I_{\theta\theta}^{ij(0001;0)})\right)\right]\right\}, \tag{A1.1}$$

$$\frac{\partial(U_s)_{max}}{\partial C_l^i} = \frac{6D}{h^2}\left\{2\eta\,\sin\theta_v\left[\theta_0\sin\theta_v\left(\sum_{j=1}^{m} C_l^j I_{ll}^{ij(0000;-1)}\right) + \left(\sum_{j=1}^{m} C_\theta^j I_{l\theta}^{ij(0010;-1)}\right)\right.\right.$$

$$\left. + \theta_0\cos\theta_v\left(\sum_{j=1}^{m} C_r^j I_{lr}^{ij(0000;-1)}\right)\right] + \frac{2\theta_0}{\eta}\left(\sum_{j=1}^{m} C_l^j I_{ll}^{ij(0101;1)}\right)$$

$$+ 2\nu\left[\left(\sum_{j=1}^{m} C_\theta^j I_{l\theta}^{ij(0110;0)}\right) + \theta_0\sin\theta_v\left(\sum_{j=1}^{m} C_l^j (I_{ll}^{ij(0100;0)} + I_{ll}^{ij(0001;0)})\right)\right.$$

$$\left. + \theta_0\cos\theta_v\left(\sum_{j=1}^{m} C_r^j I_{lr}^{ij(0100;0)}\right)\right] + (1-\nu)\left[\frac{\eta}{\theta_0}\left(\sum_{j=1}^{m} C_l^j I_{ll}^{ij(1010;-1)}\right)\right.$$

$$\left.\left. + \left(\sum_{j=1}^{m} C_\theta^j I_{l\theta}^{ij(1001;0)}\right) - \eta\,\sin\theta_v\left(\sum_{j=1}^{m} C_\theta^j I_{l\theta}^{ij(1000;-1)}\right)\right]\right\}, \tag{A1.2}$$

$$\frac{\partial(U_s)_{max}}{\partial C_r^i} = \frac{12D}{h^2}\left\{\frac{\theta_0 l_0\cos\theta_v}{R_0}\left(\sum_{j=1}^{m} C_r^j I_{rr}^{ij(0000;-1)}\right) + \frac{l_0}{R_0}\left(\sum_{j=1}^{m} C_\theta^j I_{r\theta}^{ij(0010;-1)}\right)\right.$$

$$\left. + \frac{\theta_0 l_0\sin\theta_v}{R_0}\left(\sum_{j=1}^{m} C_l^j I_{rl}^{ij(0000;-1)}\right) + \nu\theta_0\cos\theta_v\left(\sum_{j=1}^{m} C_l^j I_{rl}^{ij(0001;0)}\right)\right\}, \tag{A1.3}$$

$$\frac{\partial(U_b)_{max}}{\partial C_\theta^i} = D\left\{\frac{1}{R_0^2}\left[\frac{\eta}{\theta_0}\left(\sum_{j=1}^{m} C_\theta^j I_{\theta\theta}^{ij(1010;-3)}\right) - \frac{\eta}{\theta_0^2\cos\theta_v}\left(\sum_{j=1}^{m} C_r^j I_{\theta r}^{ij(1020;-3)}\right)\right.\right.$$

$$\left. - \tan\theta_v\left(\sum_{j=1}^{m} C_r^j I_{\theta r}^{ij(1001;-2)}\right)\right] - \frac{\nu}{R_0 l_0}\left(\sum_{j=1}^{m} C_r^j I_{\theta r}^{ij(1020;-1)}\right)$$

$$+ \frac{2(1-\nu)}{R_0}\left[\frac{\theta_0\cos\theta_v}{l_0}\left(\sum_{j=1}^{m} C_\theta^j I_{\theta\theta}^{ij(0101;-1)}\right)\right.$$

$$- \frac{\theta_0\sin\theta_v}{R_0}\left(\sum_{j=1}^{m} C_\theta^j (I_{\theta\theta}^{ij(0100;-2)} + I_{\theta\theta}^{ij(0001;-2)})\right)$$

$$\left. + \frac{\theta_0\eta\,\sin^2\theta_v}{R_0}\left(\sum_{j=1}^{m} C_\theta^j I_{\theta\theta}^{ij(0000;-3)}\right) - \frac{1}{l_0}\left(\sum_{j=1}^{m} C_r^j I_{\theta r}^{ij(0111;-1)}\right)\right.$$

$$+\frac{\tan\theta_v}{R_0}\left(\sum_{j=1}^{m} C_r^j I_{\theta r}^{ij(0110;-2)}\right)+\frac{\tan\theta_v}{R_0}\left(\sum_{j=1}^{m} C_r^j I_{\theta r}^{ij(0011;-2)}\right)$$

$$-\frac{l_0\tan^2\theta_v}{R_0^2}\left(\sum_{j=1}^{m} C_r^j I_{\theta r}^{ij(0010;-3)}\right)\Bigg]\Bigg\}, \tag{A2.1}$$

$$\frac{\partial(U_b)_{max}}{\partial C_l^i}=0 \tag{A2.2}$$

$$\frac{\partial(U_b)_{max}}{\partial C_r^i}=D\Bigg\{\frac{\eta}{R_0^2\theta_0^3\cos^2\theta_v}\left(\sum_{j=1}^{m} C_r^j I_{rr}^{ij(2020;-3)}\right)+\frac{\theta_0\sin\theta_v\tan\theta_v}{R_0 l_0}\left(\sum_{j=1}^{m} C_r^j I_{rr}^{ij(0101;-1)}\right)$$

$$-\frac{\eta}{R_0^2\theta_0^2\cos\theta_v}\left(\sum_{j=1}^{m} C_\theta^j I_{r\theta}^{ij(2010;-3)}\right)-\frac{\tan\theta_v}{R_0^2}\left(\sum_{j=1}^{m} C_\theta^j I_{r\theta}^{ij(0110;-2)}\right)$$

$$+\frac{\tan\theta_v}{R_0^2\theta_0\cos\theta_v}\left(\sum_{j=1}^{m} C_r^j (I_{rr}^{ij(2001;-2)}+I_{rr}^{ij(0120;-2)})\right)$$

$$+\frac{\theta_0}{l_0^2\eta}\left(\sum_{j=1}^{m} C_r^j I_{rr}^{ij(0202;1)}\right)+\frac{\nu}{l_0}\Bigg[-\frac{1}{R_0}\left(\sum_{j=1}^{m} C_\theta^j I_{r\theta}^{ij(0210;-1)}\right)$$

$$+\frac{1}{R_0\theta_0\cos\theta_v}\left(\sum_{j=1}^{m} C_r^j (I_{rr}^{ij(0220;-1)}+I_{rr}^{ij(2002;-1)})\right)$$

$$+\frac{\theta_0\sin\theta_v}{l_0}\left(\sum_{j=1}^{m} C_r^j (I_{rr}^{ij(0201;0)}+I_{rr}^{ij(0102;0)})\right)$$

$$+\frac{2(1-\nu)}{R_0}\Bigg[-\frac{1}{l_0}\left(\sum_{j=1}^{m} C_\theta^j I_{r\theta}^{ij(1101;-1)}\right)+\frac{\tan\theta_v}{R_0}\left(\sum_{j=1}^{m} C_\theta^j I_{r\theta}^{ij(1001;-2)}\right)$$

$$+\frac{\tan\theta_v}{R_0}\left(\sum_{j=1}^{m} C_\theta^j I_{r\theta}^{ij(1100;-2)}\right)-\frac{l_0\tan^2\theta_v}{R_0^2}\left(\sum_{j=1}^{m} C_\theta^j I_{r\theta}^{ij(1000;-3)}\right)$$

$$-\frac{\tan\theta_v}{R_0\theta_0\cos\theta_v}\left(\sum_{j=1}^{m} C_r^j (I_{rr}^{ij(1011;-2)}+I_{rr}^{ij(1110;-2)})\right)$$

$$+\frac{1}{l_0\theta_0\cos\theta_v}\left(\sum_{j=1}^{m} C_r^j I_{rr}^{ij(1111;-1)}\right)+\frac{\eta\tan^2\theta_v}{R_0\theta_0}\left(\sum_{j=1}^{m} C_r^j I_{rr}^{ij(1010;-3)}\right)\Bigg]\Bigg\}, \tag{A2.3}$$

$$\frac{\partial T_{max}}{\partial C_\theta^i} = \rho h \omega^2 \theta_0 l_0 R_0 \cos\theta_v \left(\sum_{j=1}^{m} C_\theta^j I_{\theta\theta}^{ij(0000;1)} \right), \tag{A3.1}$$

$$\frac{\partial T_{max}}{\partial C_l^i} = \rho h \omega^2 \theta_0 l_0 R_0 \cos\theta_v \left(\sum_{j=1}^{m} C_l^j I_{ll}^{ij(0000;1)} \right), \tag{A3.2}$$

$$\frac{\partial T_{max}}{\partial C_r^i} = \rho h \omega^2 \theta_0 l_0 R_0 \cos\theta_v \left(\sum_{j=1}^{m} C_r^j I_{rr}^{ij(0000;1)} \right), \tag{A3.3}$$

where the integral notation $I_{\alpha\beta}^{ij(abcd;e)}$ is given in equation (19.2).